RAA 2020 Vol. **20** No. **12**, 201(12pp) doi: 10.1088/1674-4527/20/12/201

http://www.raa-journal.org *http://iopscience.iop.org/raa*

***R**esearch in*
***A**stronomy and*
***A**strophysics*

Gamma-ray bursts with extended emission: classifications, energy correlations and radiation properties

Xiao-Lu Zhang[1], Chuan-Tao Zhang[1], Xiu-Juan Li[1], Fu-Fang Su[1,3], Xiao-Fei Dong[1], Heon-Young Chang[2] and Zhi-Bin Zhang[1⋆]

[1] College of Physics and Engineering, Qufu Normal University, Qufu 273165, China; *astrophy0817@163.com*
[2] Department of Astronomy and Atmospheric Sciences, Kyungpook National University, 1370 Sankyuk-dong, Buk-gu, Daegu 702-701, Korea
[3] Shandong Provincial Key Laboratory of Laser Polarization and Information Technology, Qufu Normal University, Qufu 273165, China

Received 2020 February 19; accepted 2020 August 6

Abstract Thanks to more and more gamma-ray bursts with measured redshift and extended emission detected by the recent space telescopes, it is urgent and possible to check whether those previous energy correlations still satisfy the particular sample involving only the bursts accompanied by tail radiations. Using 20 long and 22 short bursts with extended emission, we find that the popular γ-ray energy correlations of the intrinsic peak energy versus the isotropic energy (Amati relation) and the intrinsic peak energy versus the peak luminosity (Yonetoku relation) do exist in both short and long bursts. However, it is much better if these gamma-ray bursts with extended emissions are reclassified into two subgroups of E-I and E-II that make the above energy correlations more tight. As proposed by Zhang et al., the energy correlations can be utilized to distinguish these kinds of gamma-ray bursts in the plane of bolometric fluence versus peak energy as well. Interestingly, the peculiar short GRB 170817A belongs to the E-I group in the fluence versus peak energy plane, but it is an outlier of both the Amati and Yonetoku relations even though the off-axis effect has been corrected. Furthermore, we compare the radiation features between the extended emissions and the prompt gamma-rays in order to search for their possible connections. Taking into account all these factors, we conclude that gamma-ray bursts with extended emission are still required to model with dichotomic groups, namely E-I and E-II classes, which hint that they might have different origins.

Key words: gamma-ray burst: general — method: statistics — radiation mechanisms: non-thermal

1 INTRODUCTION

The fascinating phenomenon of gamma-ray bursts (GRBs) manifests the fastest and most dynamic astronomical events in the universe (Klebesadel et al. 1973). GRB durations (T_{90}) ranging from milliseconds to tens of minutes (Zhang et al. 2014) usually express the lasting time of prompt γ-rays (Norris et al. 1995). According to the T_{90}, GRBs have traditionally been classified into two types, namely long GRBs (LGRBs) with $T_{90} > 2$ s and short ones with $T_{90} < 2$ s (Kouveliotou et al. 1993) in the observer frame, and the bimodal distribution also exists in the rest frame (Zhang & Choi 2008). This classification criterion has been confirmed by a number of observations (Gehrels et al. 2004; Paciesas et al. 1999; Zhang et al. 2016; Zitouni et al. 2015, 2018; Tarnopolski 2019a,b) while some other authors insisted that the number of subgroups in GRBs should be three (Chattopadhyay et al. 2007; Horváth & Tóth 2016) or five (Tóth et al. 2019; Chattopadhyay & Maitra 2018). However, a special kind of GRB with an extended emission (EE) component was reported subsequently in many papers or catalogs (Mazets et al. 2004; Norris & Bonnell 2006; Kaneko et al. 2015; Svinkin et al. 2016), which was found to confuse the classification scheme of long and short GRBs (SGRBs) according to only T_{90} (Zhang et al. 2016). The EE had been thought to be produced by a relativistic wind extracting rotational energy from a protomagnetar on a timescale of 10–100 s (Metzger et al. 2008), magnetar spin-down (Zhang & Mészáros 2002; Fan & Xu 2006; Bucciantini et al. 2012), the process of fall-back accre-

⋆ Corresponding author

tion onto a newborn magnetar (Gompertz et al. 2014; Gibson et al. 2017), or a delayed energy injection causing the continued brightening of the early X-ray emissions as exhibited by GW170817/GRB 170817A (Li et al. 2018).

Many authors argued that LGRBs are formed from the collapse of massive stars associated with hypernovae (e.g., Kinugawa et al. 2019; Galama et al. 1998; Hjorth et al. 2003; Melandri et al. 2014; Fruchter et al. 2006). SGRBs are produced by the merger of either two neutron stars or a neutron star with a black hole (Gompertz et al. 2020; Li & Paczyński 1998; Fryer et al. 1999; Popham et al. 1999; Bulik et al. 1999; Troja et al. 2008; Wiggins et al. 2018). There are a number of empirical energy correlations for long bursts such as the $\tau - L_{\rm p}$ relation (Norris et al. 2000), the $V - L_{\rm p}$ relation (Fenimore & Ramirez-Ruiz 2000; Reichart et al. 2001), the $N_{peak} - L_{\rm p}$ relation (Schaefer 2003), the $\tau_{rel} - L_{\rm p}$ relation (Zhang et al. 2006, 2008), the $\tau_{RT} - L_{\rm p}$ relation (Schaefer 2007), the $E_{\rm p,i} - \tau_{RT} - L_{\rm p}$ relation (Qi & Lu 2012), the $L - T - E$ relation (Xu & Huang 2012), the Liang-Zhang relation (Liang & Zhang 2005), etc, in which the intrinsic peak energy $E_{\rm p,i} = (1+z)E_{\rm p,o}$ versus the isotropic energy $E_{\rm iso}$ (hereafter Amati relation, Amati et al. 2002) and the $E_{\rm p,i}$ versus the peak luminosity $L_{\rm p}$ (hereafter Yonetoku relation, Yonetoku et al. 2004) are two frequently-studied ones. With the increasing number of SGRBs with known redshift, people ascertained that at least parts of these above energy relations also hold for SGRBs. For example, Zhang et al. (2018) (hereafter paper I) analyzed Swift/BAT and Fermi/GBM GRB data and found that the power law indexes of both the Amati and Yonetoku relations for SGRBs are correspondingly consistent with those for long ones. This is however different from some early conclusions drawn by the limited data points of SGRBs (e.g., Amati 2006, 2012). Despite decades of studying these sorts of energy relations, the underlying emission mechanisms still remain controversial (Dainotti & Amati 2018; Ahlgren et al. 2019).

On the other hand, whether these kinds of energy relations also exist for the special EE bursts is an open question. In practice, the EE components following main peaks of a small fraction of GRBs have been identified not only in short bursts (Ioka et al. 2005; Barthelmy et al. 2005; Norris & Bonnell 2006; Li et al. 2020a,b) but also in long ones (Connaughton 2002; Bostancı et al. 2013). Moreover, Yu et al. (2020) found that SGRBs with and without EEs are diversely distributed in the plot of peak flux versus fluence, which may indicate they are triggered by different binary coalescence mechanisms. Similarly, some long bursts also have softer gamma-ray emissions with very long timescale. In recent years, more and more GRBs with softer EE tails have been detected by the Swift satellite owing to its lower energy ranges. Therefore, the primary task of the paper is to test the existent possibilities and the consistency of the Amati and Yonetoku relations of the EE bursts with those previously obtained with normal GRBs. Additionally, we shall check how to reclassify these EE bursts in a more appropriate way according to their diverse energy correlations. It is noticeable that GRB 170817A as the first gravitational-wave-associated SGRB with EE will be paid more attention in terms of its classification. Sample selection and data reduction methods are described in Section 2. Our results are presented in Section 3. We will end with conclusions in Section 4.

2 DATA AND METHODS

Firstly, we collect the GRBs with EE and redshift reported in literatures between July 2005 and August 2017 (Norris & Bonnell 2006; Gompertz et al. 2013; van Putten et al. 2014; Kaneko et al. 2015; Zhang et al. 2016; Gibson et al. 2017; Kisaka et al. 2017; Yu et al. 2020). In order to reduce the sampling selection effect, we chose not only short GRBs but also long bursts to constitute our complete GRB sample, including only EE bursts in this paper. Kisaka et al. (2017) proposed a phenomenological formula consisting of two functions to identify the EE components and identified 65 GRBs with EE, of which less than half had measured redshifts. However, some of them could not show obvious EE segments in their multi-energy bands light curves, especially in lower energy channels. To ensure reliability in sampling, we have double-checked the light curves with a criterion of signal-to-noise (S/N) larger than 2 to judge the EE segments for the EE candidates taken from literatures. In total, 42 EE GRBs with known redshift are chosen to compose our sample. Of the 42 EE bursts, 20 long and 22 short bursts are included, and 28 and 14 GRBs are respectively detected by Swift/BAT and other satellites. It happens that the EE GRB sample also consists of 20 E-I and 22 E-II bursts. Note that the E-I and E-II GRBs are not equal to the short and long ones, correspondingly (see the definition in Sect. 3.2 for details). The physical parameters are listed in Table 1, where Column (1) gives the GRB name, Column (2) lists the duration T_{90}, Column (3) expresses the cosmological redshift, Columns (4)–(6) respectively represent the observed peak energy $E_{\rm p,o}$, and two spectral indexes (α and β) of the GRB νF_ν spectrum, Columns (7) and (8) provide the observed energy fluence S_γ in units of erg cm^{-2} and peak photon flux P_γ in units of ph cm^{-2} s^{-1}, and Columns (9) and (10) show the energy bands from $E_{\rm min}$ to $E_{\rm max}$ of detectors and their corresponding K-correction factors K_c from the observer frame to the source frame in energy band

1–10 000 keV, individually. The relevant references are provided in Column (11). Finally, E-I and E-II in Column (12) list the detailed types of the EE GRBs based on the different energy correlations they exhibit.

Subsequently, we will rely on the selected sample of EE bursts to study their potential energy correlations that can be applied to classify them into different subgroups. The methods and steps are completely the same as in our previous paper I. In addition, we comparatively investigate the radiation properties of the EE components and the main peak emissions of the prompt γ-rays for distinct classes of GRBs with EE. Hopefully, we shall find some possible connections of the EE segments with their corresponding main peaks in order to explore the EE origins. For this purpose, the times and photon fluxes when the EE parts ($t_{\rm p,EE}$ and $F_{\rm p,EE}$) and the main bursts ($t_{\rm p,main}$ and $F_{\rm p,main}$) peak separately are measured and compared. Note that two peak times are recorded from the trigger time of a detector and the peak fluxes are measured for the mask-weighted light curves. Especially, two variables, $t_{\rm p,EE}$ and $F_{\rm p,EE}$, have been estimated from the lower energy channel where the EE components are usually identified and are relatively softer than the main bursts. To ensure the EE segments can be reliably measured, the selection criterion of S/N$\geq$ 3 has been adopted. In this way, we pick out 10 short and 19 long GRBs to study the relationships of timescales, intensities together with energy correlations of the EE portions. We need to point out that 10 E-I and 19 E-II bursts are also involved in this comparative study. It is however a coincidence that the numbers of different kinds of bursts are unexpectedly equal.

3 RESULT

3.1 Parameter Distributions

The redshift distributions of different EE bursts in our sample are displayed in Figure 1, where the median redshifts are z=0.71, 1.1, 0.52 and 1.29 for short, long, E-I and E-II GRBs, respectively. It is noticeable that the redshift differences between E-I and E-II GRBs are comparably larger than those between short and long bursts on the whole. Applying a Kolmogorov-Smirnov (K-S) test to the redshift distributions of short and long bursts returns the statistic $D = 0.31$ less than the critical value of $D_{\alpha'}(n_1, n_2) = 0.42$ and the *p*-value of 0.2 at a significance level $\alpha' = 0.05$ for $n_1 = 20$ and $n_2 = 22$, signifying that short and long GRBs share the same redshift distribution; while a K-S test on the redshift distributions of E-I and E-II bursts returns the statistic $D = 0.43 > D_{\alpha'}(n_1, n_2) = 0.42$ and the *p*-value of 0.03 for $\alpha' = 0.05$, which indicates that the redshifts of E-I and E-II bursts are drawn from different parent distributions.

Figure 2 displays the distributions of the low-energy spectral index of α with mean values of –0.69, –1.41, –0.70 and –1.31 and scatters of 0.58, 0.41 and 0.55 0.37 for the short, long, E-I and E-II GRBs, respectively. The K-S tests yield $D = 0.58$ and $p = 8.5\times10^{-4}$ between short and long GRBs, and $D = 0.61$ and $p = 3.7\times10^{-4}$ between E-I and E-II GRBs, which demonstrate that they all are differently distributed. In Figure 3, we compare the $E_{\rm p,o}$ distributions and get $D_{\alpha'}(n_1, n_2) = 0.26$ with $p = 0.41$ between short and long bursts and $D_{\alpha'}(n_1, n_2) = 0.66$ with $p = 7.8 \times 10^{-5}$ between E-I and E-II bursts which affirm that the observed peak energies of E-I and E-II GRBs have significantly diverse distributions. However, the $E_{\rm p,o}$ distributions of short and long GRBs are statistically the same as what some previous authors found for BATSE and Swift bursts (Ghirlanda et al. 2004; Zhang et al. 2020). The mean $E_{\rm p,o}$ values of short, long, E-I and E-II GRBs are respectively $281.8^{+55.9}_{-46.2}$, $147.9^{+38.3}_{-30.4}$, $422.7^{+18.2}_{-12.9}$ and $97.7^{+11.9}_{-10.6}$ keV. The $E_{\rm p,i}$ distributions in Figure 4 are very similar to those in Figure 3 and also show that short and long bursts are taken from the same parent distribution while E-I and E-II GRBs are distributed differently. We notice that the average $E_{\rm p,i}$ value of type E-I GRBs is still larger than that of type E-II GRBs in the rest frame. Nevertheless, the mean $E_{\rm p,i}$ values are $380.2^{+66.5}_{-46.2}$ and $346.7^{+24.8}_{-23.1}$ for short and long GRBs respectively and a K-S test gives $D_{\alpha'}(n_1, n_2) = 0.22$ with $p = 0.61$, signifying that their $E_{\rm p,i}$ distributions are uniform.

3.2 Spectrum-energy Relations

Following our paper I, we use the data in Table 1 to calculate the isotropic energy $E_{\rm iso} = 4\pi D_l^2 S_{\rm bolo}(1+z)^{-1}$ and the peak luminosity $L_{\rm p} = 4\pi D_l^2 P_{\rm bolo}$, where D_l is the cosmological distance, $S_{\rm bolo} = K_c S_\gamma$ and $P_{\rm bolo} = K_c P_\gamma$ are bolometric fluence and flux transferred from the observed fluence S_γ and flux P_γ with a *K*-correction factor of K_c respectively (paper I). Figure 5 features the Amati relations of $E_{\rm p,i} \sim C_1 E_{\rm iso}^{\eta_1}$ for the above four EE GRB groups in the rest frame. They can be individually written as

$$E_{\rm p,i} = 1783.61^{+527.5}_{-407.3}\left(\frac{E_{\rm iso}}{10^{52}\,{\rm erg}}\right)^{0.43\pm0.06}\ ({\rm keV}) \quad (1)$$

for 21 SGRBs and

$$E_{\rm p,i} = 212.82^{+32.4}_{-28.2}\left(\frac{E_{\rm iso}}{10^{52} erg\,{\rm erg}}\right)^{0.37\pm0.06}\ ({\rm keV}) \quad (2)$$

for 20 LGRBs. However, short and long GRBs are moderately overlapped and dispersedly distributed in the plane of $E_{\rm p,i}$ vs. $E_{\rm iso}$. If redividing these EE bursts into

Table 1 Physical Parameters of GRBs with EE

GRB	T_{90} (s)	z	$E_{\rm p}$ (keV)	α	β	S_γ (erg cm^{-2})	P_γ (ph cm^{-2} s^{-1})	$E_{\rm min}-E_{\rm max}$ (keV)	K_c	Ref	Type
(1)	(2)	(3)	(4)	(5)	(6)	(7)	(8)	(9)	(10)	(11)	(12)
050724⋆	96	0.257	78.91±8.0	–2.02	-	8.90×10^{-7}	3.35	15-150	5.37	[1,12]	E-II
051016B⋆	4	0.9364	20.42±5.34	–1.588	-	1.67×10^{-7}	0.685	15-350	2.26	[1,13]	E-II
051221A	1.4	0.547	402±93	–1.08	-	3.20×10^{-6}	12.1	20-2000	1.07	[4,10]	E-I
051227⋆	114.6	0.8	332.01±211.02	–1.41	-	7.09×10^{-7}	0.95	15-350	1.77	[1,3]	E-I
060306⋆	60.94	1.559	69.38±13.67	–1.254	-	2.45×10^{-6}	6.41	15-350	1.35	[1,13]	E-II
060313	0.74	1.7	837.41±438.12	–0.61	-	1.14×10^{-6}	10.85	15-350	3.68	[1,3]	E-I
060614⋆	108.7	0.125	393.02±250.96	–2.23	-	1.88×10^{-5}	11.39	15-350	7.84	[1,3]	E-II
060801⋆	0.49	1.13	620.22±342.95	0.28	-	7.84×10^{-8}	0.75	15-350	3.47	[1,3]	E-I
060814⋆	145.3	0.84	302.37±127.18	–1.412	-	2.39×10^{-5}	8.38	15-350	1.72	[1,13]	E-II
061006⋆	129.9	0.4377	664±227	–0.62	-	3.57×10^{-6}	5.3	20-10000	1.01	[5,12]	E-I
061201	0.76	0.111	873±458	–0.36	-	5.32×10^{-6}	3.55	20-3000	1.02	[6,12]	E-I
061210⋆	85.3	0.41	544.04±309.56	–1.56	-	1.10×10^{-6}	2.78	15-350	2.20	[1,12]	E-I
070223⋆	100	1.6295	54.44±14.45	–1.48	-	1.98×10^{-6}	0.491	15-350	1.57	[1,13]	E-II
070506⋆	4.3	2.31	55.12±11.29	–0.768	-	2.22×10^{-7}	0.948	15-350	1.24	[1,13]	E-II
070714B⋆	64	0.92	164.87±73.13	–1.15	-	7.23×10^{-7}	2.75	15-350	1.31	[1,3]	E-II
070724A	0.4	0.457	82±5	–1.15	-	3.00×10^{-8}	0.94	15-150	1.56	[7,12]	E-I
071227⋆	1.8	0.383	1000±100	–0.7	-	1.60×10^{-6}	1.68	20-1000	1.64	[8,12]	E-I
080123⋆	115	0.495	44.93±4.49	–1.99	-	5.52×10^{-7}	1.43	15-350	2.63	[1,12]	E-II
080603B⋆	60	2.69	74.94±10.86	–1.21	-	2.98×10^{-6}	4.72	15-350	1.32	[1,13]	E-II
080905A⋆	1	0.128	311.2±100	0.12	–2.35	8.51×10^{-7}	6.32	10-1000	1.51	[1,12]	E-I
080905B⋆	128	2.374	256.10±65.06	–1.579	–2.29	2.75×10^{-6}	1.03	15-350	1.80	[1,13]	E-II
090426⋆	1.2	2.609	55.09±27	–1.11	-	1.76×10^{-7}	2	15-150	1.49	[1,9]	E-II
090510⋆	0.3	0.903	4302±483.2	–0.86	–2.58	3.37×10^{-6}	40.95	10-1000	3.94	[2,11]	E-I
090530⋆	40.46	1.266	92.14±30.56	–1.078	-	1.33×10^{-6}	3.68	15-350	1.23	[1,13]	E-II
090927⋆	2.2	1.37	61.95±19.12	–1.301	-	2.97×10^{-7}	1.85	15-350	1.4	[1,13]	E-II
100117A	0.3	0.915	327.22±52.91	–0.1	–6.3	9.26×10^{-8}	0.96	10-1000	1.02	[1,2]	E-I
100625A	0.33	0.452	482.13±61.93	–0.59	-12.24	2.32×10^{-7}	2.54	10-1000	1.12	[1,2]	E-I
100704A⋆	197.5	3.6	381.75±80.77	–1.655	-2	8.91×10^{-6}	5.1	15-350	2.05	[1,13]	E-II
100724A	1.4	1.288	42.5±15.18	–0.51	-	1.41×10^{-7}	1.56	15-150	1.29	[1,12]	E-II
100814A⋆	174.5	1.44	312.96±188.9	–1.331	–2.44	1.47×10^{-5}	3.05	15-350	1.7	[1,13]	E-II
100906A⋆	114.4	1.727	138.37±36.45	–1.722	–1.86	1.89×10^{-5}	11.1	15-350	1.84	[1,13]	E-II
101219A	0.6	0.718	490±103	–0.22	-	3.60×10^{-6}	4.2	20-10000	1.01	[9,10]	E-I
111117A	0.47	2.211	370±37	–0.69	-	6.70×10^{-7}	2.8	15-150	3.84	[1,10]	E-I
120804A⋆	0.81	1.3	116.18±39.82	–0.97	-	8.66×10^{-7}	10.64	15-350	1.19	[1,3]	E-II
131004A⋆	1.54	0.71	118.1±29.7	–1.36	-22.09	5.09×10^{-7}	9.82	10-1000	1.17	[1,2]	E-II
150120A	1.2	0.46	130±50	–1.43	–1.65	4.17×10^{-7}	4.94	10-1000	2.31	[1,2]	E-II
150423A	0.22	1.39	120±35	0.43	-	6.30×10^{-8}	2.6	15-150	1.42	[1,12]	E-I
150424A	91	0.3	47.06±6.64	–0.49	–2.19	1.50×10^{-6}	12	10-1000	1.12	[1,2]	E-II
160410A⋆	8.2	1.717	495.3±232.9	–1.11	-	1.15×10^{-6}	0.34	15-350	2.07	[1,3]	E-I
160624A	0.2	0.483	1168±546.5	–0.63	–3.65	1.21×10^{-7}	6.39	10-1000	1.84	[1,2]	E-I
160821B⋆	0.48	0.16	46.32±5.38	–0.12	-	1.03×10^{-7}	1.68	15-150	1.19	[1,2]	E-I
170817A⋆	2.05	0.009783	214.7±56.6	–0.60	-	2.79×10^{-7}	3.73	10-1000	1.00	[2,12]	E-I

[1] *https://swift.gsfc.nasa.gov/results/batgrbcat/*; [2] *https://heasarc.gsfc.nasa.gov/W3Browse/fermi/fermigtrig.html*; [3] *http://butler.lab.asu.edu*; [4] Golenetskii et al. (2005); [5] Golenetskii et al. (2006a); [6] Golenetskii et al. (2006b); [7] Golenetskii et al. (2006c); [8] Golenetskii et al. (2007); [9] Goldstein et al. (2010); [10] Fong et al. (2015); [11] Razzaque (2010); [12] Goldstein et al. (2017); Zhang et al. (2018); [13] Zhang et al. (2016). Star symbols indicate those GRBs with brighter EE components at a level of S/N$\geq$ 3.

E-I and E-II subgroups as featured in the lower panel of Figure 5, one can obtain two more tight Amati relations with smaller standard deviations to be

$$E_{\rm p,i} = 2062.76^{+552.9}_{-436.0}\left(\frac{E_{\rm iso}}{10^{52}\,{\rm erg}}\right)^{0.45\pm0.05}\ ({\rm keV}) \quad (3)$$

for 19 E-I GRBs and

$$E_{\rm p,i} = 207.60^{+23.5}_{-21.1}\left(\frac{E_{\rm iso}}{10^{52}\,{\rm erg}}\right)^{0.36\pm0.04}\ ({\rm keV}) \quad (4)$$

for 22 E-II GRBs, which conversely verifies that the E-I/II classification could be more physical. It is noteworthy that GRB 170817A has not been utilized during the above fits. All the fitting parameters are listed in Table 2 where one can find that the power-law indexes are marginally consistent with each other and the energy correlations of short and long bursts are much closer to those of E-I and II GRBs. In addition, the fitted η_1 values are surprisingly coincident with those obtained by paper I for 31 short and 252 long GRBs with lower $E_{\rm p,o}$ mainly observed by Swift/BAT, but slightly smaller than the previous value of $\eta_1 \simeq 0.5$ (e.g. Amati et al. 2002; Amati 2006; Amati et al. 2019). This hints that the Amati relation might evolve with the peak energy. In particular, we find that the peculiar

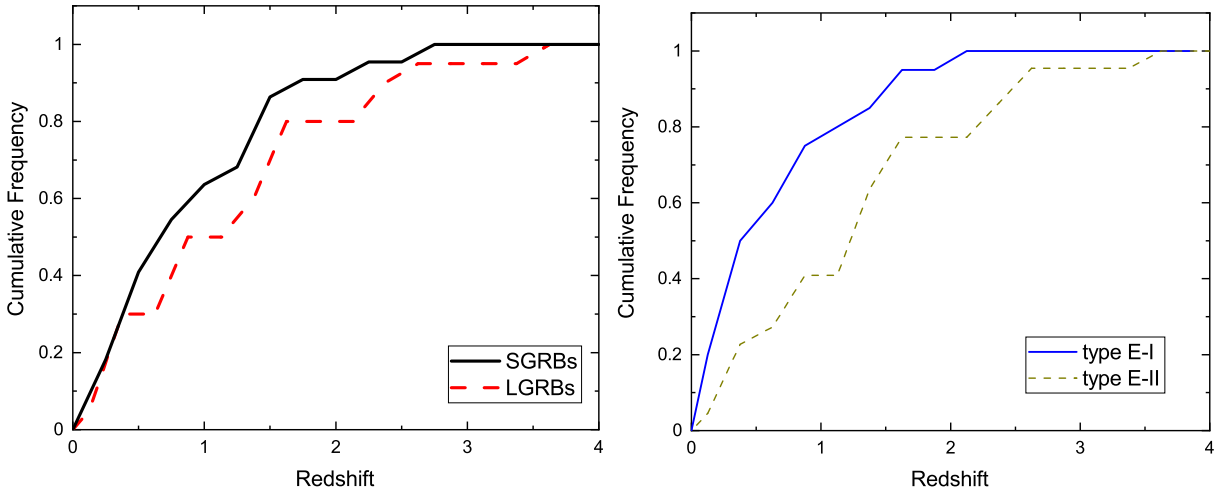

Fig. 1 *Left panel*: Cumulative probability distributions of redshifts for short (*solid line*) and long (*dashed line*) EE GRBs. *Right panel*: Cumulative probability distributions of redshifts for E-I (*solid line*) and E-II (*dashed line*) GRBs with EE.

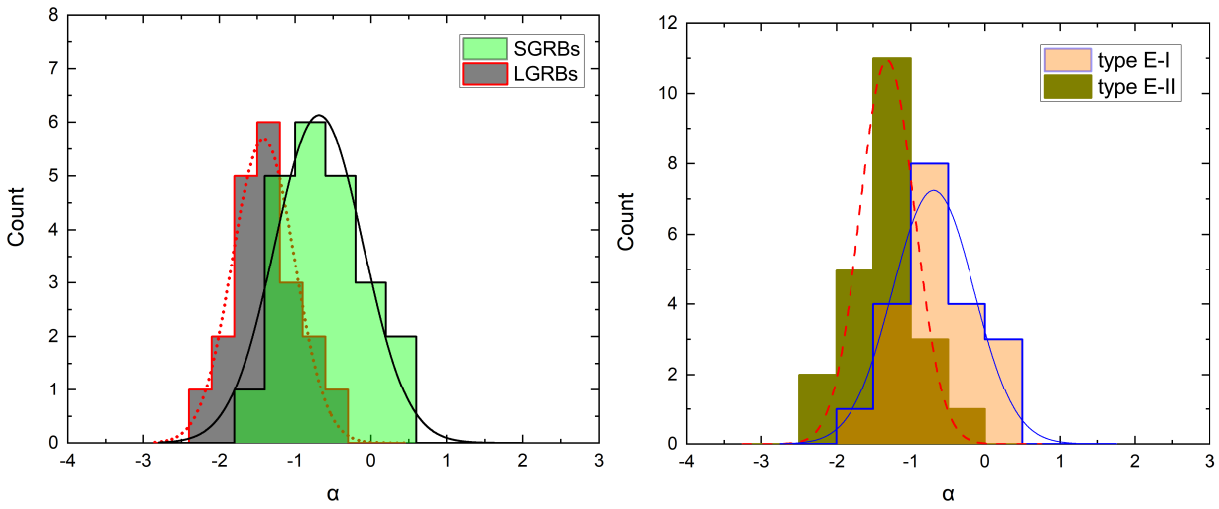

Fig. 2 *Left panel*: Distributions of low-energy spectral index of α in Band function for short (*green*) and long (*gray*) GRBs. *Right panel*: Distributions of low-energy spectral index of α in Band function for E-I (*light orange*) and E-II (*dark yellow*) GRBs. The different lines are the best fits to the histograms with a Gaussian function.

GRB 170817A always violates the newly built Amati relations even though the off-axis effect has been corrected according to the method adopted by Zou et al. (2018). To perform the off-axis corrections for GRB 170817A, we adopt the viewing angle of θ_v= 0.53 radians, the half-opening jet angle $\theta_j = 0.1$ radians from Hajela et al. (2019) and the initial Lorentz factor $\Gamma = 8$ (Salafia et al. 2018). Its on-axis energies are $E_{\rm p,i,on} = 2713.4 \pm 715.3$ keV and $E_{iso,on} = (9.23 \pm 0.56) \times 10^{48}$ erg that are correspondingly about one order of magnitude larger than the those estimated by Zou et al. (2018), where $\Gamma = 13.4$ and $\theta_v = 0.175$ radians had been assumed.

Similarly, we try to fit the Yonetoku relations $E_{\rm p,i} \sim C_2 L_{\rm p}^{\eta_2}$ of the above four kinds of EE GRBs in Figure 6 and their corresponding formulas are written as

$$E_{\rm p,i} = 464.13^{+82.9}_{-70.3} \left(\frac{L_{\rm p}}{10^{51}\,{\rm erg\,s^{-1}}}\right)^{0.42\pm0.05} ({\rm keV}), \quad (5)$$

$$E_{\rm p,i} = 138.11^{+20.7}_{-18.0} \left(\frac{L_{\rm p}}{10^{51}\,{\rm erg\,s^{-1}}}\right)^{0.37\pm0.07} ({\rm keV}), \quad (6)$$

$$E_{\rm p,i} = 516.00^{+86.2}_{-73.9} \left(\frac{L_{\rm p}}{10^{51}\,{\rm erg\,s^{-1}}}\right)^{0.44\pm0.05} ({\rm keV}), \quad (7)$$

$$E_{\rm p,i} = 128.05^{+13.7}_{-12.4} \left(\frac{L_{\rm p}}{10^{51}\,{\rm erg\,s^{-1}}}\right)^{0.37\pm0.05} ({\rm keV}) \quad (8)$$

for short, long, E-I and E-II EE GRBs, respectively. We are aware that the power-law indexes of the four kinds of bursts are approximately consistent with each other as

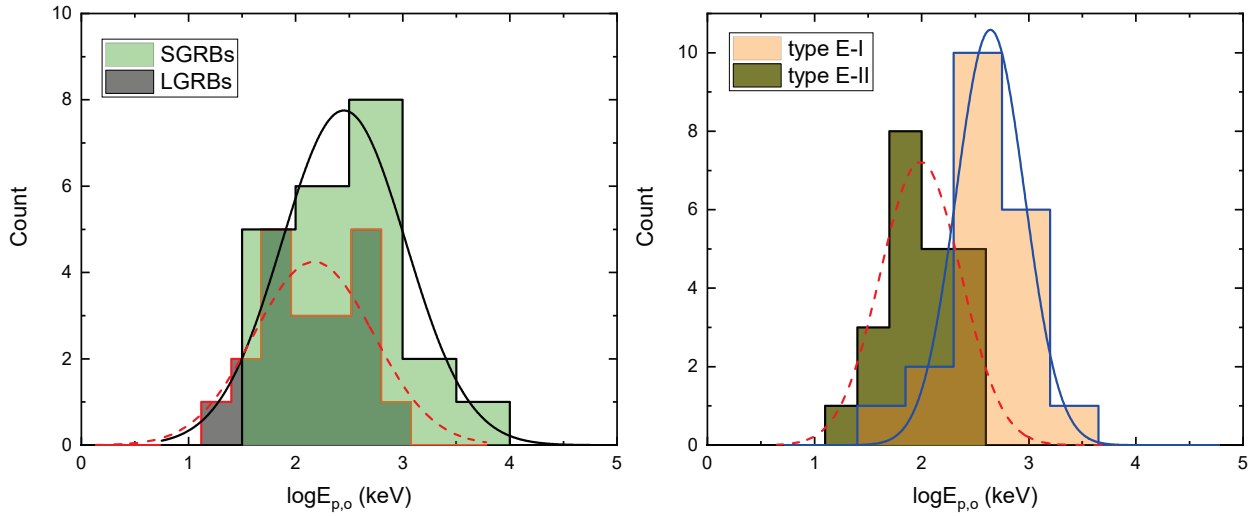

Fig. 3 *Left panel*: Distributions of $E_{\rm p,o}$ in Band function for short (*green*) and long (*gray*) GRBs. *Right panel*: Distributions of $E_{\rm p,o}$ in Band function for E-I (*light orange*) and E-II (*dark yellow*) GRBs. The distinct lines are the best fits to the histograms with a lognormal function.

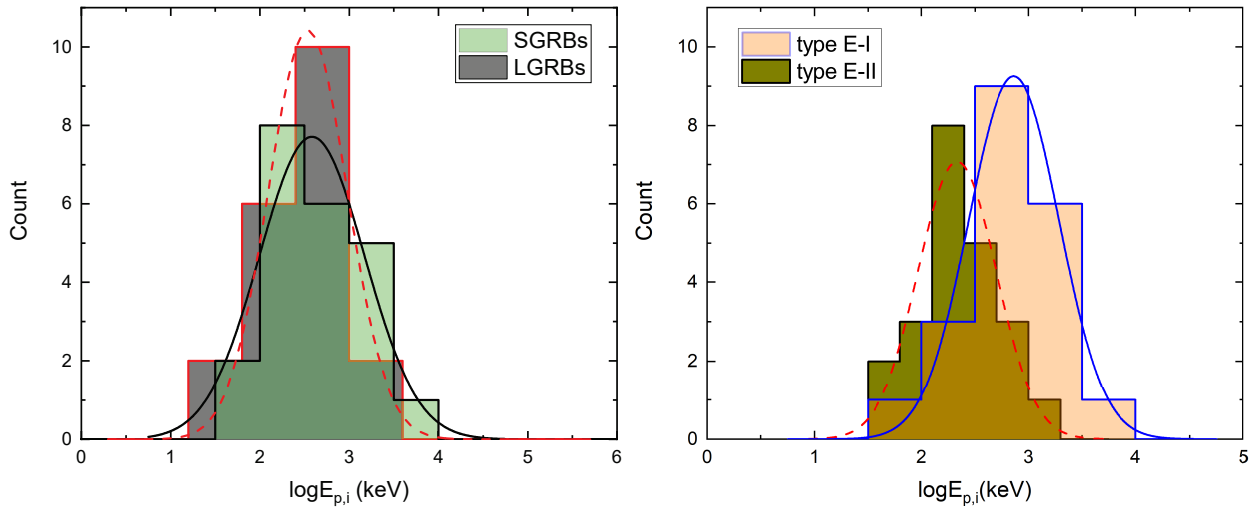

Fig. 4 *Left panel*: Distributions of the intrinsic peak energy of $E_{\rm p,i}$ for short (*green*) and long (*gray*) GRBs. *Right panel*: Distributions of the intrinsic peak energy of $E_{\rm p,i}$ for E-I (*light orange*) and E-II (*dark yellow*) GRBs. The distinct lines are the best fits to the histograms with a lognormal function.

shown in Table 2 and they are slightly less than 0.5 which demonstrates the synchrotron radiation to be dominant for the GRBs with EE (see also Zhang et al. 2012, 2018). Our results are roughly in agreement with some previous ones (Wei & Gao 2003; Yonetoku et al. 2004; Wang et al. 2011; Zhang et al. 2012, 2018). No matter whether the off-axis viewing effect is corrected, GRB 170817A is undoubtedly a violator of the Yonetoku relation as illustrated in Figure 6. After taking into account the same off-axis parameters, one can obtain the on-axis peak luminosity of GRB 170817A to be $L_{\rm p,on} = (1.68 \pm 0.36) \times 10^{49}$ erg s^{-1} dimmer than most GRBs.

3.3 Classifying GRBs with Energy Correlations

We now apply our new energy correlations expressed in Equations (1)-(8) to verify if they can distinguish different kinds of GRBs in the plane of $E_{\rm p,o}$ versus $S_{\rm bolo}$. If substituting $E_{\rm iso} = 4\pi D_l^2 S_{\rm bolo}(1+z)^{-1}$ (or $L_{\rm p} = 4\pi D_l^2 P_{\rm bolo}$) into $E_{\rm p,i} = C_1(E_{\rm iso}/10^{52}{\rm erg})^{\eta_1}$ (or $E_{\rm p,i} = C_2(L_{\rm p}/10^{51}{\rm erg\,s^{-1}})^{\eta_2}$) and carrying out variable separations, one can arrive at the energy ratios $\zeta_j = E_{\rm p,o}^{1/\eta_j}/S_{\rm bolo} \propto A_j(z)(j = 1, 2)$ evolving with redshift as displayed in Figure 7, in which $A_j(z)$ will reach its maximum values at a certain redshift of $z_{\rm p}$ (see also paper I for details). Table 2 lists the values of $z_{\rm p}$ and $A(z_{\rm p})$ constrained with the fitted parameters C_j and

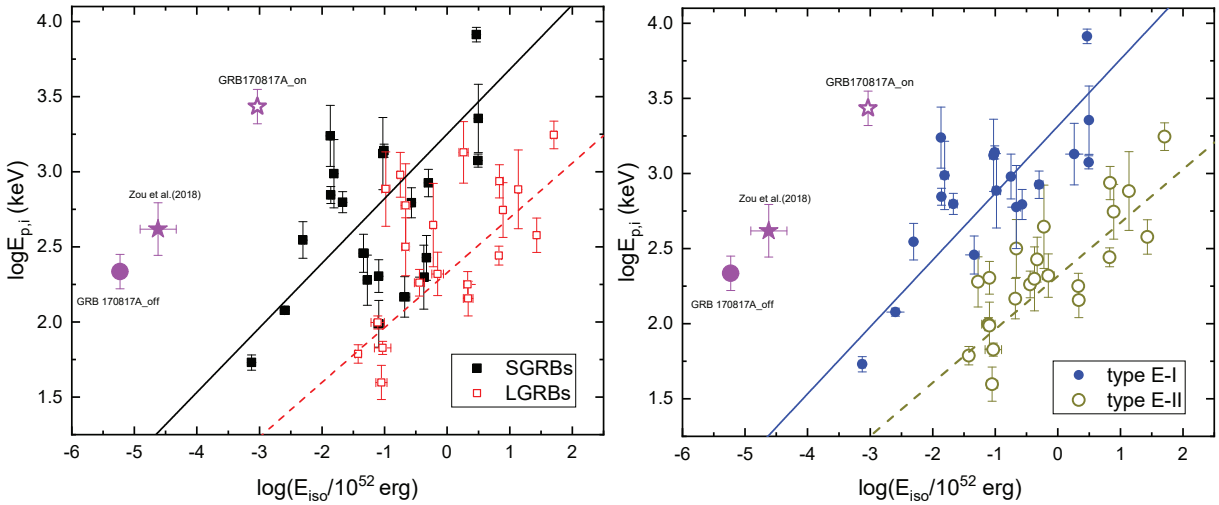

Fig. 5 The energy relations of $E_{\rm p,i}$ versus $E_{\rm iso}$ on a logarithmic scale for short (*filled squares*) and long (*empty squares*) GRBs in the *left panel* and for E-I (*filled circles*) and E-II (*empty circles*) GRBs in the *right panel*. The straight lines stand for the best fits to data. For the peculiar SGRB 170817A, the filled large circle represents the off-axis measurements, while the on-axis parameters given by Zou et al. (2018) and this work are signified by the filled and the empty stars, respectively (see text for details).

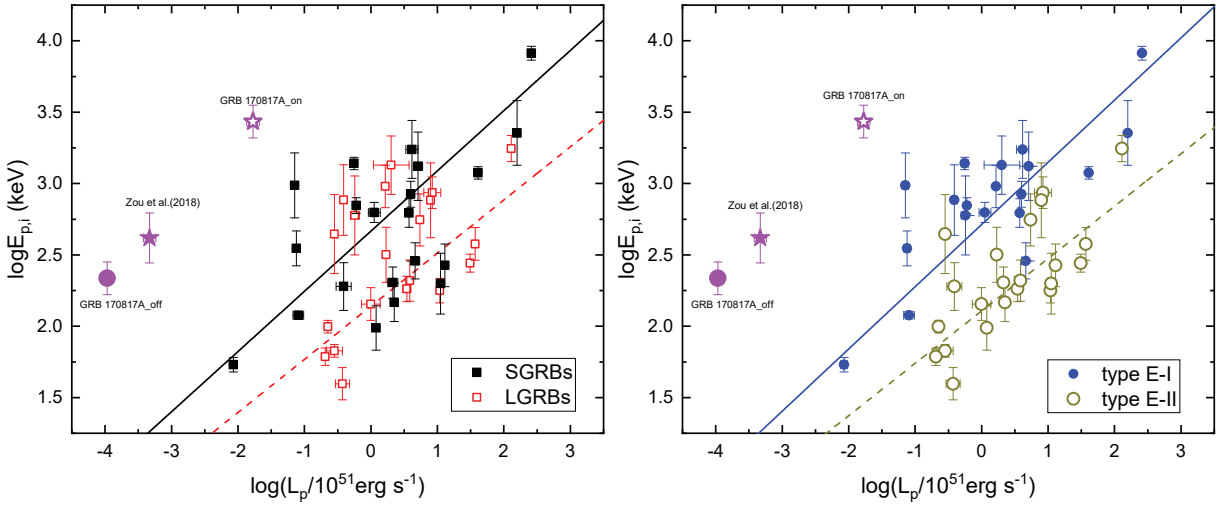

Fig. 6 The energy relations of $E_{\rm p,i}$ versus $L_{\rm p}$ on a logarithmic scale for short and long GRBs in the *left panel* and for E-I and E-II GRBs in the *right panel*. All symbols are the same as in Fig. 5. The straight lines stand for the best fits to data.

Table 2 Parameters of Energy Correlations for the EE GRBs

Type	Correlation	C (keV)	η	R^b	$z_{\rm p}$	$A_{z_{\rm p}}$
SGRB (N=21^a)	$E_{\rm p,i}-E_{\rm iso}$	$1783.61^{+527.5}_{-407.3}$	0.43 ± 0.06	0.73	2.7	2.98×10^{12}
SGRB (N=21^a)	$E_{\rm p,i}-L_{\rm p}$	$464.13^{+82.9}_{-70.3}$	0.42 ± 0.05	0.74	2.6	1.61×10^{12}
LGRB (N=20)	$E_{\rm p,i}-E_{\rm iso}$	$212.82^{+32.4}_{-28.2}$	0.37 ± 0.06	0.66	2.0	1.19×10^{11}
LGRB (N=20)	$E_{\rm p,i}-L_{\rm p}$	$138.11^{+20.7}_{-18.0}$	0.37 ± 0.07	0.62	2.0	3.00×10^{11}
E-I (N=19^a)	$E_{\rm p,i}-E_{\rm iso}$	$2062.76^{+552.9}_{-436.0}$	0.45 ± 0.05	0.80	3.0	2.18×10^{12}
E-I (N=19^a)	$E_{\rm p,i}-L_{\rm p}$	$516.00^{+86.2}_{-73.9}$	0.44 ± 0.05	0.80	2.9	1.29×10^{12}
E-II (N=22)	$E_{\rm p,i}-E_{\rm iso}$	$207.60^{+23.5}_{-21.1}$	0.36 ± 0.04	0.75	1.9	1.31×10^{11}
E-II (N=22)	$E_{\rm p,i}-L_{\rm p}$	$128.05^{+13.7}_{-12.4}$	0.37 ± 0.05	0.73	2.0	2.58×10^{11}

[a] The short and off-axis GRB 170817A/GW 170817 has not been utilized during our fits. [b] R index is the linear correlation coefficient of these energy relations on a logarithmic scale.

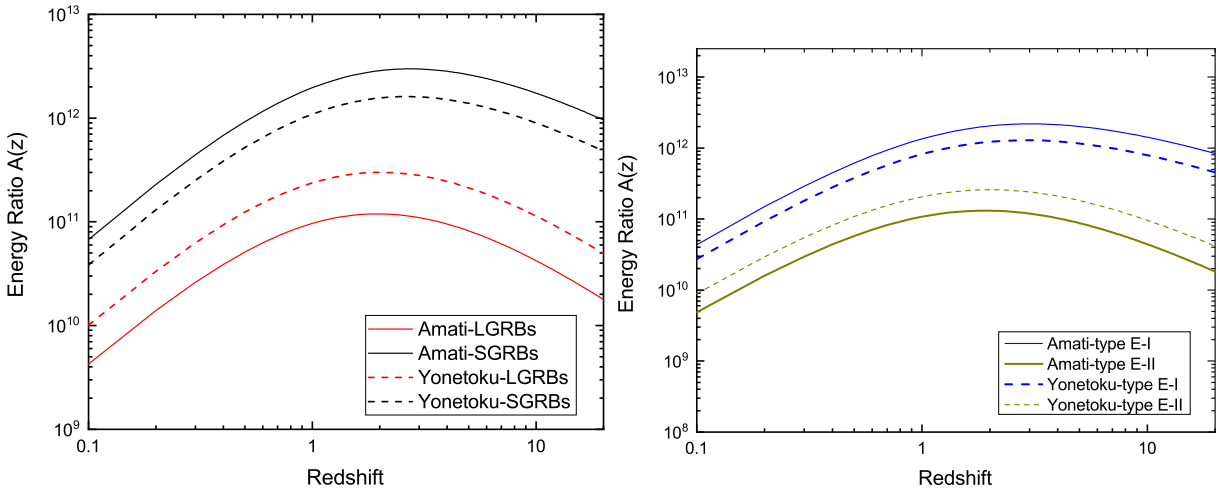

Fig. 7 The dependencies of $A(z)$ on redshift are considered for the Amati (*solid lines*) and Yonetoku (*dashed lines*) relations of short and long GRBs in the *left panel*, and the same two energy relations of E-I and E-II GRBs in the *right panel*.

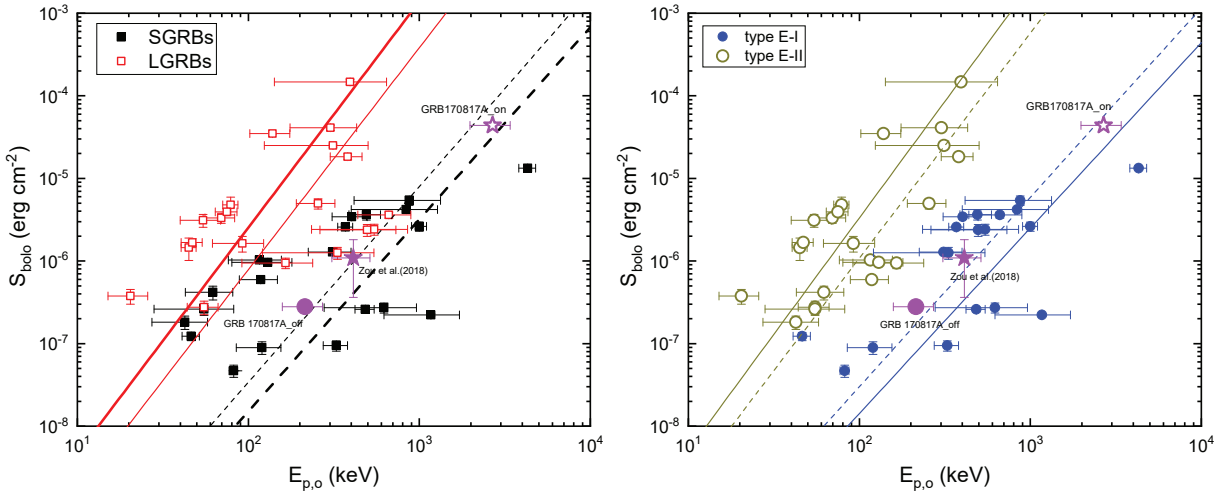

Fig. 8 The $S_{\rm bolo}$ is plotted against the $E_{\rm p,o}$ for different types of bursts. The lower limits on the $S_{\rm bolo}$-$E_{\rm p,o}$ relationship from the Amati/Yonetoku relations of short (*thick/thin black dashed line*) versus long (*thick/thin red solid line*) GRBs and those of E-I (*thick/thin blue dashed line*) versus E-II (*thick/thin dark yellow solid line*) bursts are individually presented in the *left* and *right* panels respectively. All symbols are the same as in Fig. 5.

η_j from Equation (1) to Equation (8). This in turn puts a lower limit on the logarithmic relationships of $\log S_{\rm bolo} \geq \log E_{\rm p,o}/\eta_j - \log A(z_{\rm p})$ as displayed in Figure 8, where we find that both the Amati and Yonetoku relations can be utilized to classify these EE GRBs themselves, which is very similar to the findings for all the GRB samples in paper I. To draw the lower limit lines from the Yonetoku relations, $P_{\rm bolo} = S_{\rm bolo}(P_\gamma/S_\gamma) \simeq S_{\rm bolo}/T_{90}$ with a typical duration $T_{90} = 2$ s has been applied. Previously, Qin & Chen (2013) also proposed that GRBs are better to be sorted into Amati and non-Amati classes. Note that the non-Amati bursts in Qin & Chen (2013) actually correspond to the SGRBs. Interestingly, these empirical energy correlations are available to identify not only short vs. long but also E-I vs. E-II GRBs. By contrast, the E-I/II classification scheme is more reasonable since the two kinds of bursts are less overlapped. Although GRB 170817A matches neither the Amati nor Yonetoku relations, we need to emphasize that GRB 170817A is always located near to the region of either the short or E-I GRBs as seen from Figures 5, 6 and 8, regardless of whether the off-axis effect is considered or not.

3.4 Spectral Hardness

As depicted in Figure 9, the $E_{\rm p,o}$ and T_{90} are weakly anti-correlated with a Pearson correlation coefficient of $\rho = -0.16$ and a chance probability of 0.4. Interestingly, the E-II bursts tend to have longer T_{90} but smaller $E_{\rm p,o}$

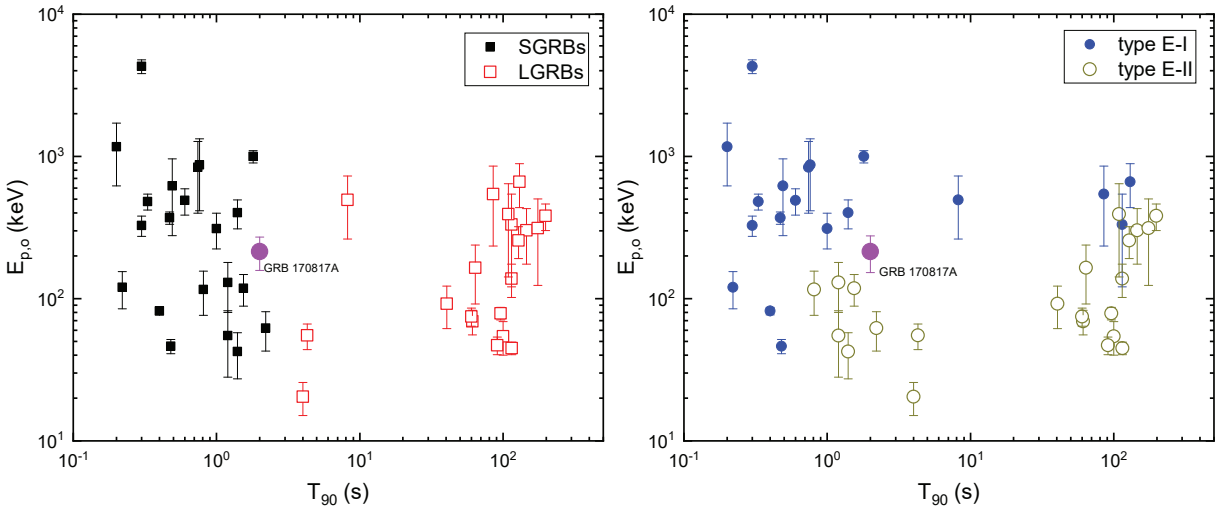

Fig. 9 Correlations between T_{90} and $E_{\rm p,o}$ for short and long GRBs in the *left panel* and for E-I and E-II GRBs in the *right panel*. All symbols are the same as in Fig. 5. GRB 170817A, viewed off-axis, is marked with a larger filled circle.

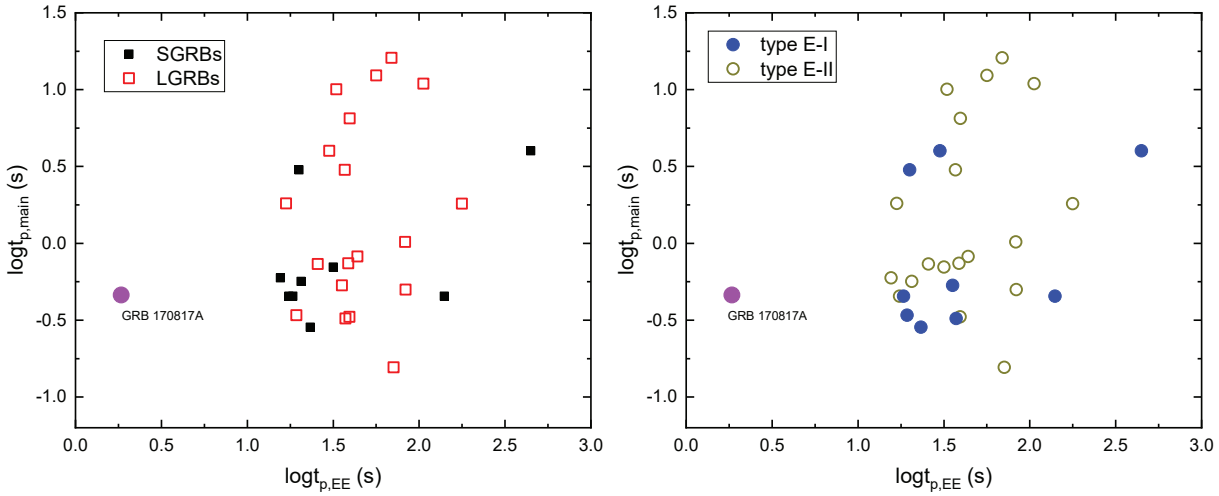

Fig. 10 Correlations between the peak time of main bursts ($t_{\rm p,main}$) and that of the EE components ($t_{\rm p,EE}$) on a logarithmic scale for short (*filled squares*) and long (*empty squares*) GRBs in the *right panel* and for E-I (*filled circles*) and E-II (*empty circles*) GRBs in the *left panel*. GRB 170817A viewed off-axis is marked with a larger filled circle.

in contrast with the E-I GRBs and both of them exhibit a wider T_{90} span from 0.1 to 200 s. On the contrary, the $E_{\rm p,o}$ does not show an obvious dependence on the T_{90} from short to long bursts, which is consistent with some results of BATSE and Swift normal GRBs (e.g. Ghirlanda et al. 2004; Zhang et al. 2020). It happens that GRB 170817A just lies on the boundaries between short/E-I and long/E-II GRBs, which makes it more mysterious in the aspects of classification.

3.5 Properties of the EE Components

In case of the EE component, it also contains many useful parameters that can be utilized to unveil the associations of the central engine with the EE formation mechanisms including the energy injection effect (Yu & Huang 2013; Xu & Huang 2015). In this section, we will focus on the comparative studies of the time delay, peak brightness and peak luminosity of the EE segments for 10 short and 19 long GRBs (see those bursts marked with a star in Table 1) with well-determined EEs at a higher confidence level of S/N$>$ 3. Coincidentally, there are 10 E-I and 19 E-II bursts in the selected sub-sample. In addition, the energy correlations of the EE parts will be also investigated to explore the possible connections with the GRB counterparts.

Figure 10 indicates that there are no correlations between the peak time of main bursts ($t_{\rm p,main}$) and the peak time of the EE components ($t_{\rm p,EE}$). Except for GRB 170817A with an extremely early EE, the majority of GRBs have EE profiles peaking at a delay time of

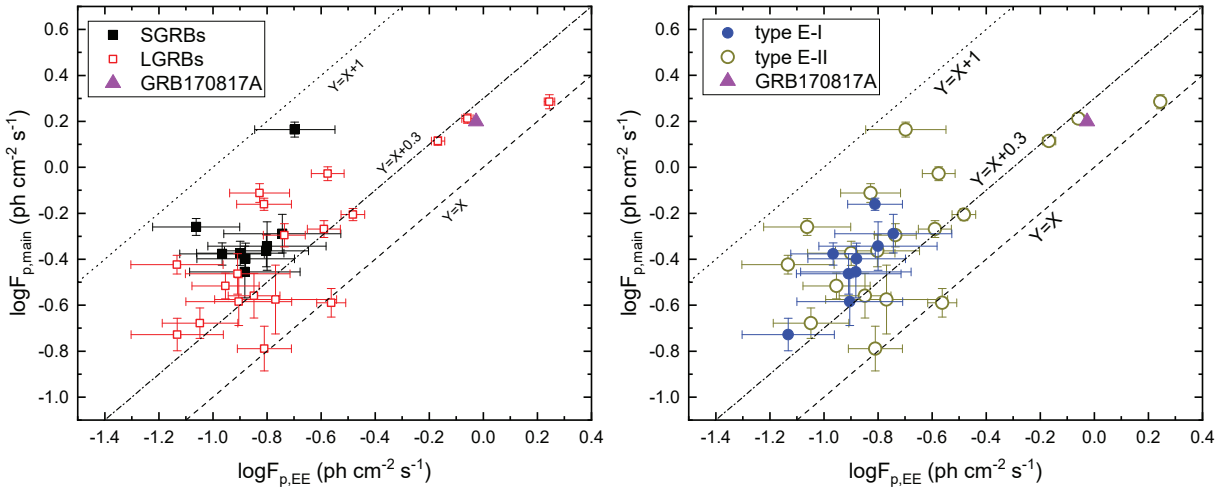

Fig. 11 Correlation of the peak flux of main bursts ($F_{\rm p,main}$) with that of the EE components ($F_{\rm p,EE}$) on a logarithmic scale. All symbols are the same as in Fig. 10. GRB 170817A viewed off-axis is marked with a larger filled triangle. Three peak flux ratios of $F_{\rm p,EE}$ to $F_{\rm p,main}$ are signified by the dashed, dash-dotted and dotted lines for 1, 1/2 and 1/10, respectively.

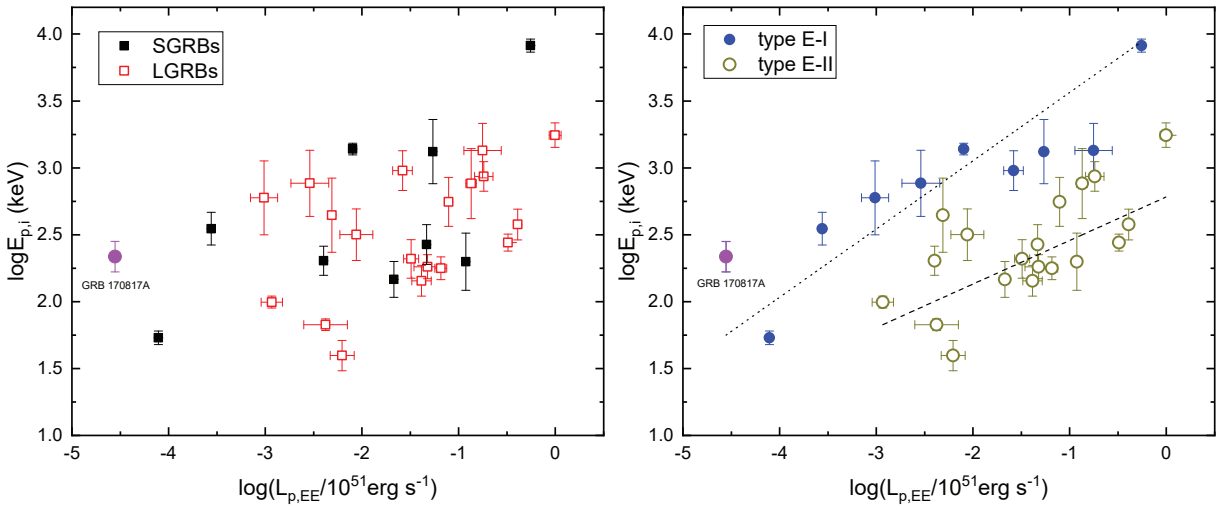

Fig. 12 The energy correlations of the $E_{\rm p,i}$ with the $L_{\rm p,EE}$ on a logarithmic scale. All symbols are the same as in Fig. 10. GRB 170817A viewed off-axis is marked with a larger filled circle. The dashed and dotted lines represent the best weighted fits to E-I and E-II GRBs in each with a power-law form (see text for details).

$45.7^{+37.5}_{-20.6}$ s after the trigger. We examine the associations of the peak fluxes of the EE components ($F_{\rm p,EE}$) with those of the main bursts ($F_{\rm p,main}$) in Figure 11, from which one gains the logarithmic correlation coefficients ρ =0.48, 0.82, 0.81 and 0.72 with p-values of 0.19, 2.1×10^{-5}, 7.3×10^{-3} and 5.7×10^{-4} for short, long, E-I and E-II GRBs, correspondingly. These correlations imply that the EE energy outputs should depend on the amount of energy in their own main bursts. There are three bursts (GRB 060614, 070223 and 100814A) with stronger EEs comparable to their main peaks. It also can be seen from Figure 11 that a large fraction of the EE GRBs have peak flux ratios of $F_{\rm p,EE}/F_{\rm p,main}$ ranging from 1/10 to 1/2. Figure 12 is plotted to test whether the popular Yonetoku relation exists during the EE phase. To do this, the EE peak luminosity is estimated by $L_{\rm p,EE} = 4\pi D_l^2 F_{\rm p,EE}$. The average $L_{\rm p,EE}$ values are $\sim 1.1\times10^{49}$ erg s^{-1} with a spread of 2.28 dex and $\sim 3.1\times10^{49}$ erg s^{-1} with a spread of 1.76 dex for short and long GRBs respectively; while the average $L_{\rm p,EE}$ values are $\sim 7.6\times10^{48}$ erg s^{-1} with a spread of 2.58 dex and $\sim 3.7\times10^{49}$ erg s^{-1} with a spread of 1.58 dex for E-I and E-II GRBs, respectively. We can find that the $L_{\rm p,EE}$ is positively correlated with the $E_{\rm p,i}$ for all kinds of EE bursts, especially for the E-I/II bursts. Interestingly, the Yonetoku relations of E-I and E-II GRBs can be individually described by $E_{\rm p,i}\propto L_{\rm p,EE}^{0.51\pm0.05}$ and $E_{\rm p,i}\propto L_{\rm p,EE}^{0.33\pm0.06}$ which are good in agreement with Equations (7) and (8) respectively. This confirms again that

the EE components should be physically associated with the prompt GRBs (see also Li et al. 2020b).

4 CONCLUSIONS

We have selected a complete sample of GRBs with EE to study their parameter properties and the possible connections between the softer EE components and the harder GRBs. Simultaneously, we checked whether some previous energy correlations still hold for these particular bursts and how to use the newly built energy correlations to classify this kind of EE burst. Our major findings of this work are summarized below:

* Unlike short and long GRBs, the redshift distributions of E-I and E-II bursts are found to arise from different parent distributions. The redshift distributions of E-I and E-II GRBs are different and their medians are 0.51 and 1.29, respectively.
* The spectral peak energies in the observer and the source frames are identically distributed for short and long bursts but differently distributed for E-I and E-II GRBs, of which their mean $E_{\rm p,o}$ values are correspondingly $\sim$422.7 keV and $\sim$97.7 keV.
* We find that the Amati and Yonetoku energy correlations do exist for not only short and long EE bursts but also E-I and E-II GRBs. By contrast, the $E_{\rm p,i}$-$E_{\rm iso}$ and $E_{\rm p,i}$-$L_{\rm p}$ power-law relations of E-I and E-II bursts are tighter than those of short and long ones. In addition, the power-law indexes of these energy relations are marginally consistent with most previous values of normal GRBs.
* Particularly, we notice that GRB 170817A as the first gravitational-wave associated SGRB with EE does not obey either the Amati or the Yonetoku relations no matter whether it was viewed off-axis or on-axis. However, GRB 170817A is located among the region of short or E-I bursts in the $E_{\rm p,o}$ versus $S_{\rm bolo}$ plot.
* It is confirmed again that the EE GRBs can be identified by the diverse Amati and Yonetoku correlations in the $E_{\rm p,o}$-$S_{\rm bolo}$ plane, which is similar to the conclusion in paper I for ordinary GRBs. Furthermore, E-I and E-II GRBs can be clearly distinguished according their different Amati or Yonetoku energy relations, redshift distributions and peak energy distributions, which demonstrate that the classification scheme of E-I and E-II bursts is more reasonable.
* Most EE segments in our sample are found to peak at a time of $45.7^{+37.5}_{-20.6}$ s after trigger occurrence which is not related with the peak time of main bursts. However, peak fluxes of the EE components and the GRBs are strongly correlated with each other. Surprisingly, we find that the $E_{\rm p,i}$ of GRBs and the EE peak luminosity of E-I/II bursts are also tightly connected with the coincident power-law indexes like those fitted by only the normal GRBs.

On the basis of these comparative studies, we conclude that it is much better to reclassify the bursts with EE into two subgroups, which are type E-I and type E-II, respectively. Therefore, we hope that the most important role of our results could reveal new insights into the physics of the EE GRBs together with their mysterious progenitors, especially on how to classify or find more EE GRBs resembling the attractive but challenging GRB 170817A.

Acknowledgements We appreciate the referee for the constructive suggestions and comments that improved the paper greatly. We thank Y. Zhang and K. Zhang for their helpful discussions. This work was supported by the Youth Innovations and Talents Project of Shandong Provincial Colleges and Universities (Grant No. 201909118) and the Natural Science Foundation (Grant Nos. ZR2018MA030, XKJJC201901 and OP201511). HYC was supported by a National Research Foundation of Korea Grant funded by the Korean government (NRF2018R1D1A3B070421880 and 2018R1A6A1A06024970).

References

Ahlgren, B., Larsson, J., Valan, V., et al. 2019, ApJ, 880, 76
Amati, L., Frontera, F., Tavani, M., et al. 2002, A&A, 390, 81
Amati, L. 2006, MNRAS, 372, 233
Amati, L. 2012, in International Journal of Modern Physics Conference Series, Vol. 12, International Journal of Modern Physics Conference Series, 19
Amati, L., D'Agostino, R., Luongo, O., Muccino, M., & Tantalo, M. 2019, MNRAS, 486, L46
Barthelmy, S. D., Cannizzo, J. K., Gehrels, N., et al. 2005, ApJL, 635, L133
Bostancı, Z. F., Kaneko, Y., & Göğüş, E. 2013, MNRAS, 428, 1623
Bucciantini, N., Metzger, B. D., Thompson, T. A., & Quataert, E. 2012, MNRAS, 419, 1537
Bulik, T., Belczyński, K., & Zbijewski, W. 1999, MNRAS, 309, 629
Chattopadhyay, T., Misra, R., Chattopadhyay, A. K., & Naskar, M. 2007, ApJ, 667, 1017
Chattopadhyay, S., & Maitra, R. 2018, MNRAS, 481, 3196
Connaughton, V. 2002, ApJ, 567, 1028
Dainotti, M. G., & Amati, L. 2018, PASP, 130, 051001
Fan, Y.-Z., & Xu, D. 2006, MNRAS, 372, L19
Fenimore, E. E., & Ramirez-Ruiz, E. 2000, arXiv e-prints, arXiv:0004176

Fruchter, A. S., Levan, A. J., Strolger, L., et al. 2006, Nature, 441, 463
Fryer, C. L., Woosley, S. E., & Hartmann, D. H. 1999, ApJ, 526, 152
Galama, T. J., Vreeswijk, P. M., van Paradijs, J., et al. 1998, Nature, 395, 670
Gehrels, N., Chincarini, G., Giommi, P., et al. 2004, ApJ, 611, 1005
Ghirlanda, G., Ghisellini, G., & Celotti, A. 2004, A&A, 422, L55
Gibson, S. L., Wynn, G. A., Gompertz, B. P., & O'Brien, P. T. 2017, MNRAS, 470, 4925
Gompertz, B. P., O'Brien, P. T., Wynn, G. A., & Rowlinson, A. 2013, MNRAS, 431, 1745
Gompertz, B. P., O'Brien, P. T., & Wynn, G. A. 2014, MNRAS, 438, 240
Gompertz, B. P., Levan, A. J., & Tanvir, N. R. 2020, ApJ, 895, 58
Hajela, A., Margutti, R., Alexander, K. D., et al. 2019, ApJL, 886, L17
Hjorth, J., Sollerman, J., Møller, P., et al. 2003, Nature, 423, 847
Horváth, I., & Tóth, B. G. 2016, Ap&SS, 361, 155
Ioka, K., Kobayashi, S., & Zhang, B. 2005, ApJ, 631, 429
Kaneko, Y., Bostancı, Z. F., Göğüş, E., & Lin, L. 2015, MNRAS, 452, 824
Kinugawa, T., Harikane, Y., & Asano, K. 2019, ApJ, 878, 128
Kisaka, S., Ioka, K., & Sakamoto, T. 2017, ApJ, 846, 142
Klebesadel, R. W., Strong, I. B., & Olson, R. A. 1973, ApJL, 182, L85
Kouveliotou, C., Meegan, C. A., Fishman, G. J., et al. 1993, ApJL, 413, L101
Li, B., Li, L.-B., Huang, Y.-F., et al. 2018, ApJL, 859, L3
Li, L.-X., & Paczyński, B. 1998, ApJL, 507, L59
Li, X.-J., Zhang, Z.-B., Zhang, C.-T., et al. 2020a, ApJ, 892, 113
Li, X. J., Zhang, Z. B., Zhang, X. L., et al., 2020b, ApJS, in Press
Liang, E., & Zhang, B. 2005, ApJ, 633, 611
Mazets, E. P., Aptekar, R. L., Frederiks, D. D., et al. 2004, in ASPC Series, 312, Gamma-Ray Bursts in the Afterglow Era, eds. M. Feroci, F. Frontera, N. Masetti, & L. Piro, 102
Melandri, A., Pian, E., D'Elia, V., et al. 2014, A&A, 567, A29
Metzger, B. D., Quataert, E., & Thompson, T. A. 2008, MNRAS, 385, 1455
Norris, J. P., Bonnell, J. T., Nemiroff, R. J., et al. 1995, ApJ, 439, 542
Norris, J. P., Marani, G. F., & Bonnell, J. T. 2000, ApJ, 534, 248
Norris, J. P., & Bonnell, J. T. 2006, ApJ, 643, 266
Paciesas, W. S., Meegan, C. A., Pendleton, G. N., et al. 1999, ApJS, 122, 465
Popham, R., Woosley, S. E., & Fryer, C. 1999, ApJ, 518, 356
Qi, S., & Lu, T. 2012, ApJ, 749, 99
Qin, Y.-P., & Chen, Z.-F. 2013, MNRAS, 430, 163
Reichart, D. E., Lamb, D. Q., Fenimore, E. E., et al. 2001, ApJ, 552, 57
Salafia, O. S., Ghisellini, G., Ghirlanda, G., & Colpi, M. 2018, A&A, 619, A18
Schaefer, B. E. 2003, ApJL, 583, L71
Schaefer, B. E. 2007, ApJ, 660, 16
Svinkin, D. S., Frederiks, D. D., Aptekar, R. L., et al. 2016, ApJS, 224, 10
Tarnopolski, M. 2019a, ApJ, 887, 97
Tarnopolski, M. 2019b, ApJ, 870, 105
Tóth, B. G., Rácz, I. I., & Horváth, I. 2019, MNRAS, 486, 4823
Troja, E., King, A. R., O'Brien, P. T., Lyons, N., & Cusumano, G. 2008, MNRAS, 385, L10
van Putten, M. H. P. M., Lee, G. M., Della Valle, M., Amati, L., & Levinson, A. 2014, MNRAS, 444, L58
Wang, F.-Y., Qi, S., & Dai, Z.-G. 2011, MNRAS, 415, 3423
Wei, D. M., & Gao, W. H. 2003, MNRAS, 345, 743
Wiggins, B. K., Fryer, C. L., Smidt, J. M., et al. 2018, ApJ, 865, 27
Xu, M., & Huang, Y. F. 2012, A&A, 538, A134
Xu, M., & Huang, Y.-F. 2015, RAA (Research in Astronomy and Astrophysics), 15, 986
Yonetoku, D., Murakami, T., Nakamura, T., et al. 2004, ApJ, 609, 935
Yu, Y.-B., & Huang, Y.-F. 2013, RAA (Research in Astronomy and Astrophysics), 13, 662
Yu, Y. B., Li, L. B., Li, B., Geng, J. J., & Huang, Y. F. 2020, New Astron., 75, 101306
Zhang, B., & Mészáros, P. 2002, ApJ, 581, 1236
Zhang, B.-B., Zhang, B., Murase, K., Connaughton, V., & Briggs, M. S. 2014, ApJ, 787, 66
Zhang, Z.-B., Deng, J.-G., Lu, R.-J., & Gao, H.-F. 2006, ChJAA (Chin. J. Astron. Astrophys.), 6, 312
Zhang, Z. B., & Choi, C. S. 2008, A&A, 484, 293
Zhang, Z.-B., Xie, G.-Z., & Choi, C.-S. 2008, International Journal of Modern Physics D, 17, 1391
Zhang, Z. B., Chen, D. Y., & Huang, Y. F. 2012, ApJ, 755, 55
Zhang, Z.-B., Yang, E.-B., Choi, C.-S., & Chang, H.-Y. 2016, MNRAS, 462, 3243
Zhang, Z. B., Zhang, C. T., Zhao, Y. X., et al. 2018, PASP, 130, 054202 (Paper I)
Zhang, Z. B., Jiang, M., Zhang, Y., et al. 2020, ApJ, 902, 40
Zitouni, H., Guessoum, N., Azzam, W. J., & Mochkovitch, R. 2015, Ap&SS, 357, 7
Zitouni, H., Guessoum, N., AlQassimi, K. M., & Alaryani, O. 2018, Ap&SS, 363, 223
Zou, Y.-C., Wang, F.-F., Moharana, R., et al. 2018, ApJL, 852, L1